Geophys. J. Int. (2005) **162,** 36–48 doi: 10.1111/j.1365-246X.2005.02632.x

Palaeomagnetism and $^{40}Ar/^{39}Ar$ geochronology of mafic dykes from the eastern Bushveld Complex (South Africa)

S. Letts,[1] T. H. Torsvik,[1,2] S. J. Webb,[1] L. D. Ashwal,[1] E. A. Eide[3] and G. Chunnett[4]

[1]*School of Geosciences, Private Bag* 3, *University of the Witwatersrand, WITS,* 2050, *South Africa*
[2]*Geological Survey of Norway, Leiv Eirikssonsvei* 39, N-7491 *Trondheim; and Institute for Petroleum Technology and Applied Geophysics, NTNU,* N-7491 *Trondheim, Norway. E-mail: trond.torsvik@ngu.no*
[3]*Geological Survey of Norway, Leiv Eirikssonsvei* 39, N-7491 *Trondheim, Norway*
[4]*Anglo Platinum,* PO Box 62179, *Marshalltown,* 2107, *South Africa*

Accepted 2005 March 8. Received 2005 February 19; in original form 2004 July 20

SUMMARY

We report palaeomagnetic and $^{40}Ar/^{39}Ar$ age data for dykes that intrude the ∼2 Ga eastern Bushveld Igneous Complex (BIC). The dykes were previously assumed to be of Karroo age (Jurassic ∼ 180 Ma) based on their NE–SW orientation. Palaeomagnetic data (pole position 8.7°N, 22°E; $dp/dm = 18/20.6°$), however, clearly demonstrate that these dykes are Precambrian in age, either ∼1.9 Ga and close to the Early Proterozoic Bushveld age, or 1649 ± 10 Ma based on $^{40}Ar/^{39}Ar$ plagioclase laser fusion ages from one of the dykes. Both normal and reverse polarity dykes are identified, and a positive reversal test together with a semi-conclusive contact test attests to a primary magnetization. If the $^{40}Ar/^{39}Ar$ age represents a primary cooling age then palaeomagnetic poles from South Africa (Kalahari) at ∼1.9 to ∼2 Ga and ∼1650 Ma are virtually identical, and suggest an apparent polar wander loop; alternatively, the Kalahari Craton drifted from high southerly (>50°) to high northerly latitudes (or vice versa) during this interval. Conversely, if we assign a ∼1.9 Ga age for dyke emplacement as suggested from a comparison with Kalahari palaeomagnetic poles (e.g. Waterberg–Soutpansberg pole), the ∼1650 Ma $^{40}Ar/^{39}Ar$ age must relate to a thermal disturbance that did not erase the primary magnetic signature.

Key words: Bushveld, dykes, geochronology, palaeomagnetism, Precambrian.

1 INTRODUCTION

The Bushveld Igneous Complex (BIC), covering an area of ∼60 000 km^2 in northern South Africa, is the world's largest layered mafic intrusion, and contains the majority of the world's resources of platinum group elements (PGE), chromium and vanadium (Lee 1996). With the current increasing world demand for PGE, there is active exploration for and exploitation of new magmatically hosted PGE deposits, especially in the Eastern and Northern Lobes of the Complex (Fig. 1). Any new mining ventures must take cognisance of geologically complicating factors that serve to disrupt the continuity of PGE-bearing horizons—these include faults and dykes, the orientations and extents of which must be known as precisely as possible.

Regional aeromagnetic data available from the South African government and proprietary high-resolution surveys (made available by Anglo Platinum) reveal that the area to the east of the BIC is riddled with dykes (Fig. 1). These dykes penetrate the mafic, PGE-rich units of the BIC. Historically, aeromagnetic data have played an important role in the exploration and exploitation of the BIC, as well as of the huge gold deposits of the Witwatersrand basin. The presence of highly magnetic Fe-Ti oxide-rich horizons in the BIC Upper Zone (Molyneux 1970; Ashwal *et al.* 2000; Maré *et al.* 2001), which can be used as marker horizons throughout large regions of the BIC, makes this method particularly useful. However, the interpretation of magnetic data in the BIC is complicated by the presence of strong remanent magnetization both in the mafic cumulate rocks and in younger dykes. Fortunately, the palaeomagnetic and petrophysical properties of the BIC have been well studied (Hattingh 1986a,b,c, 1989; Hattingh & Pauls 1994).

2 DYKES

The abundant dykes that penetrate and surround the 2.058 Ga ± 0.8 Ma BIC (Buick *et al.* 2001) are not well characterized. Ages and orientations of major dyke swarms were summarized by Hunter & Reid (1987) and Uken & Watkeys (1997) for the whole of southern Africa, but data in the region around the eastern BIC are sparse. Major periods of mafic dyke emplacement in southern Africa are associated with the Karroo (∼180 Ma), Pilanesberg (∼1.2–1.3 Ga) and Waterberg–Soutpansberg (∼1.9 Ga) magmatic events (Hanson *et al.* 2004).

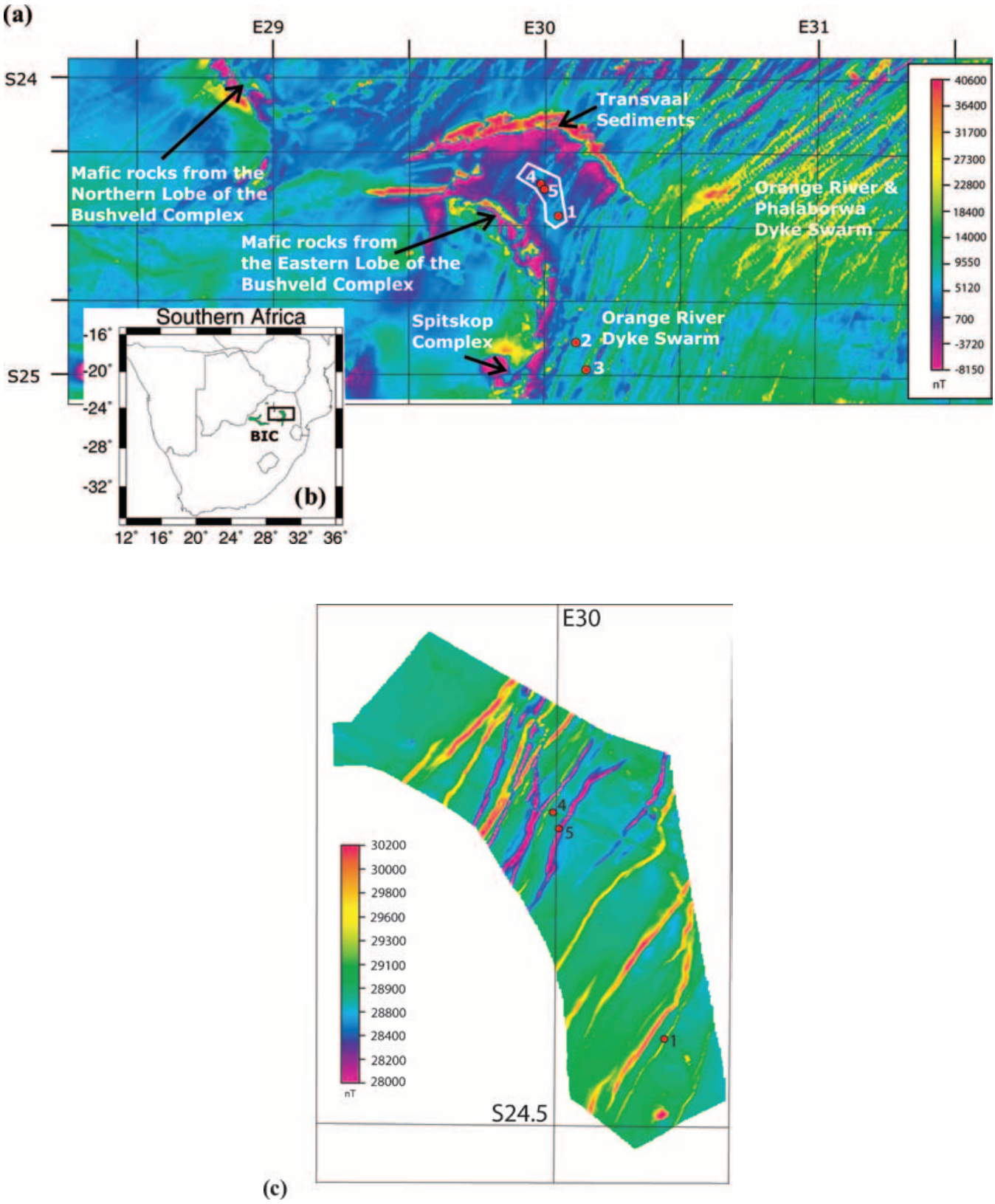

Figure 1. (a) Regional aeromagnetic map over the eastern Bushveld Complex and surrounding area, indicating locations of palaeomagnetic drill sites (1 to 5). The location of the high-resolution survey in (c) is indicated with white outlines and covers sites 1, 4 and 5. (b) Map of South Africa in which the areal extent of the aeoromagnetic map in (a) is shown as a rectangle. (c) Example of high-resolution aeromagnetic data (made available by Anglo Platinum) used to target dykes (sites 1, 4 and 5 within this survey area) and for potential field modelling (reported elsewhere).

An examination of these dyke swarms and their relationship to major mafic magmatic events in the Kaapvaal craton reveals that dyke swarms have repeatedly utilized certain emplacement directions (Uken & Watkeys 1997). Therefore, for magnetic modelling, assumptions about petrophysical properties based solely on strike direction or trend (with assumed ages) can lead to erroneous modelling of magnetic data.

The extensive Jurassic Karroo dykes and related lavas have been well-characterized palaeomagnetically (e.g. Hargraves *et al.* 1997). Far fewer data are available, however, for older dyke swarms, including those of the Pilanesberg event.

3 GEOLOGY

The study area is located in the Critical Zone of the Rustenburg Layered Suite of the eastern Bushveld Complex (Fig. 1). The majority of the area consists of medium- to coarse-grained norite and anorthosite; it is also host to the economically significant PGE deposits of the UG-2 chromite layer and the Merensky Reef (von Gruenewaldt *et al.* 1985).

A number of highly fractured and weathered dolerite dykes with a NE–SW trend have been found in the area. Individual dykes in the Bushveld Complex have not been well characterized, and the majority of dykes have been assumed to be of Karroo age (∼180 Ma) (Uken & Watkeys 1997). However, a comparison of incompatible elements (Nb, Zr, TiO_2) versus magnesium number (Mg no. = 100Mg/[Mg+Fe]) and incompatible element ratios shows that the studied dykes are not similar in composition to those of the Karroo (Eales *et al.* 1984). We conducted a palaeomagnetic and geochronological study of one subset of the Bushveld dykes to establish their ages. We will demonstrate that the dykes are not of Karroo age but instead are Proterozoic. Detailed studies in geochemistry and geochronology are needed to determine if the dykes are in fact actually related to the older Waterberg (Strauss 1947; Sharpe 1981; Hanson *et al.* 2004) and Soutpansberg (Crow & Condie 1990) magmatic events, but this is beyond the scope of this paper.

4 SAMPLING AND LABORATORY EXPERIMENTS

The natural remanent magnetization (NRM) was measured on a JR5A spinner magnetometer in a low-magnetic-field environment at the Geological Survey of Norway in Trondheim (Table 1). Susceptibility was measured on a Bartington MS2 system, whilst Curie temperatures were determined with the use of an *in-house* translation bridge. Stability of the NRM was tested by thermal demagnetization using a MM-TD-60 furnace, and, to a lesser extent, alternating field (AF) demagnetization with the use of an *in-house* two-axis tumbler demagnetizer (Figs 2–7). Characteristic remanence components (ChRc) were calculated by means of principal component analysis (Fig. 8).

A primary purpose of the project was to determine the ratio between remanent and induced magnetization (Konigsberger ratio = Q) in order to aid modelling of magnetic data (reported elsewhere). NRM data and bulk susceptibility are listed in Table 1, and, except for one dyke, Q values are very high (∼4–37). Within-site NRM directions from the dykes are also reasonably clustered and show dual polarity (*cf.* α_{95} in Table 1; Fig. 8a). Conversely, the country rocks from each site show very scattered NRM directions. The directional scatter of the host rock samples is mainly due to the presence of large and unstable grains of magnetite in the norite samples. ChRc high unblocking (HB) components for each dyke, the mean for normal polarity and reversed polarity dykes, and a combined mean for all dykes are listed in Table 2. Dykes designated normal or reversed polarity correspond to dykes associated with positive or negative magnetic anomalies (Fig. 1c). Owing to severe surface weathering, only five palaeomagnetic drilling sites were selected on excavated roads, road cuttings and river exposures (Fig. 1; detailed below).

4.1 Site 1 (dolerite dyke and host norite)

Site 1 includes a dolerite dyke cropping out on Makkubu Hill (Hackney Farm). The dyke is ∼10 m wide and is extremely fresh. The contact is not exposed and the host Bushveld norite was sampled 5 m away from the dyke. The dyke shows minor, but randomly oriented, low unblocking (LB) components. The HB component of the dyke shows a steep upward-pointing inclination (negative) with a southerly declination (Table 2; Figs 2 and 8b; dyke 1, samples 9a and 6a). Maximum unblocking temperatures are of the order of 565–580°C and with AF stability up to 70–80 mT (Fig. 2). Individual norite samples can display well-defined HB components (Fig. 2) but are very scattered at site level. This is a characteristic feature of most of the host samples.

Table 1. Mean NRM, bulk susceptibility and Konigsberger ratio (Q) of the five dykes and their host rock (except for site 2).

Site	Location (Lat., Long.)	Strike/dip (dyke) Magmatic layering	N	NRM Dec.	NRM Inc.	α_{95}	NRM (mA m^{-1})	±1σ	Sus. ($\times 10^{-6}$ SI)	±1σ	Q	±1σ
1 Dyke	24° 27′ 42″S 30° 03′ 05″E	315/unknown	8	212	−73	6.2	3387	1225	17288	9502	9.6	2.8
Host		345/15SW	6	098	−28	53.9	267	192	429	12.6	28.4	20.9
2 Dyke	24° 56′ 57″S 30° 09′ 06″E	040/80SE	9	138	−71	3.8	4282	447	30184	1507	6.4	0.5
Host		202/10S										
3 Dyke	24° 52′ 57″S 30° 07′ 00″E	010/vertical	5	006	−79	19.1	690	31	10473	5988	3.6	1.6
Host		329/16SW	11	085	−6	38	59	91	341.8	43.2	8.4	13.4
4 Dyke	24° 21′ 50″S 29° 59′ 50″E	035/68SE	3	343	84	19.1	431	18	24154	1525	0.7	0
Host		327/15SW	3	336	−16	55.3	7	3	270.8	22.4	1.2	0.5
5 Dyke	24° 22′ 15″S 30° 00′ 03″E	038/70SE	6	012	65	13.6	22138	1041	27114	6297	36.8	13.7
Host		328/16SW	5	088	42	180	613	414	568	145	53.6	44.6

N = Number of samples, Dec. = declination, Inc. = inclination, Sus. = Susceptibility.

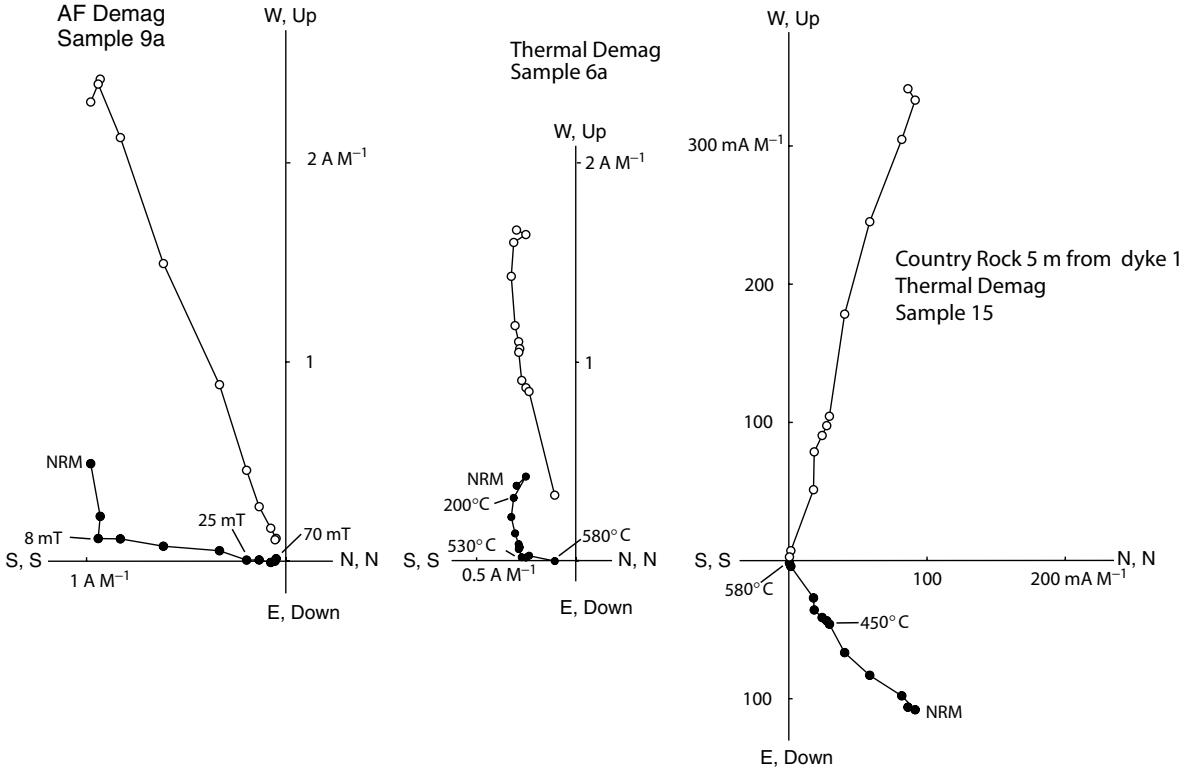

Figure 2. AF and thermal demagnetization of dyke 1 samples and a norite sample located 5 m from the dyke. The solid circles indicate points in the horizontal plane, while open circles denote points in the vertical plane. The numbers on the curves indicate temperature or AF field depending on the demagnetization method.

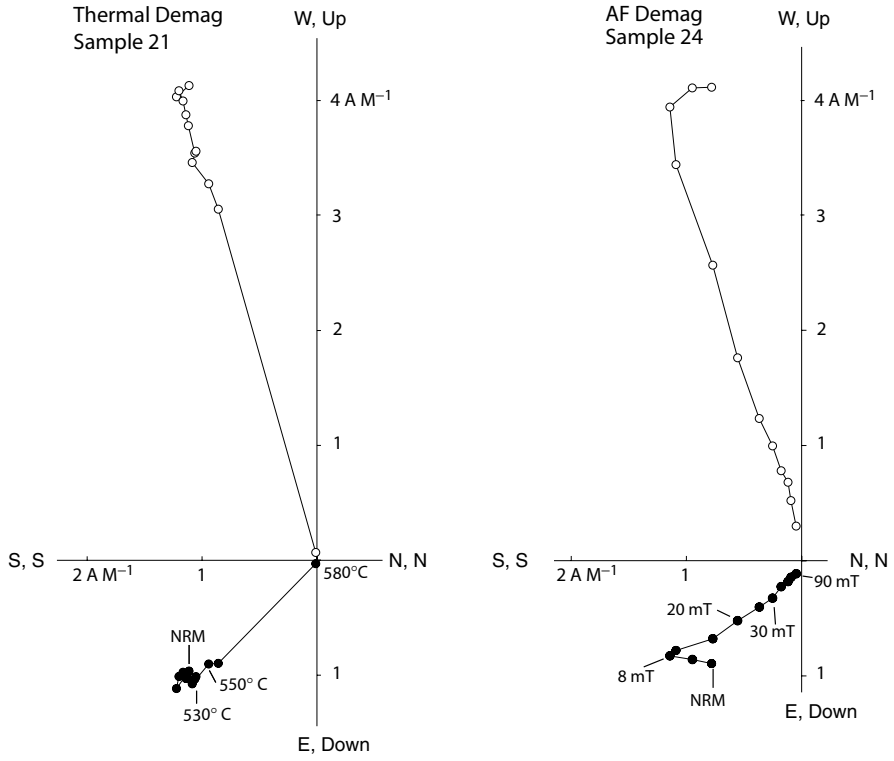

Figure 3. AF and thermal demagnetization of dyke 2 samples.

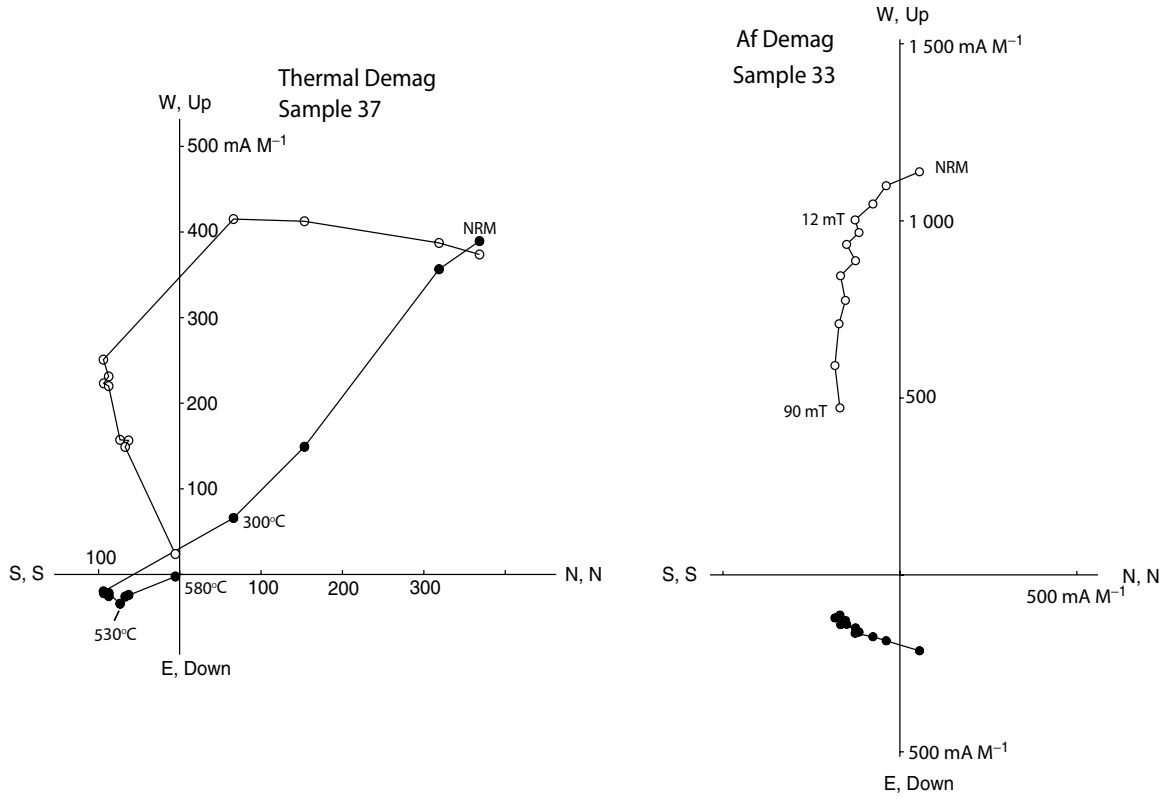

Figure 4. Thermal and AF demagnetization of dyke 3 samples. Note that the maximum available alternating field of 90 mT (900 Oe) was not sufficient to demagnetize sample 33.

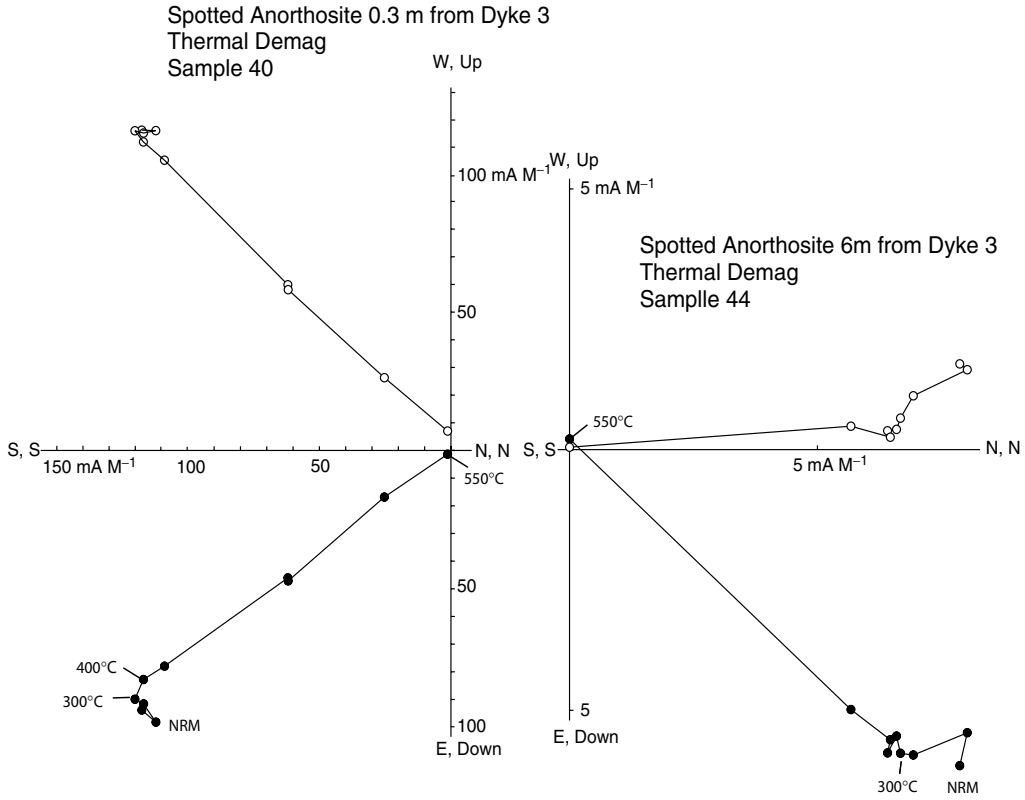

Figure 5. Thermal demagnetization of the surrounding spotted anorthosite next to dyke 3.

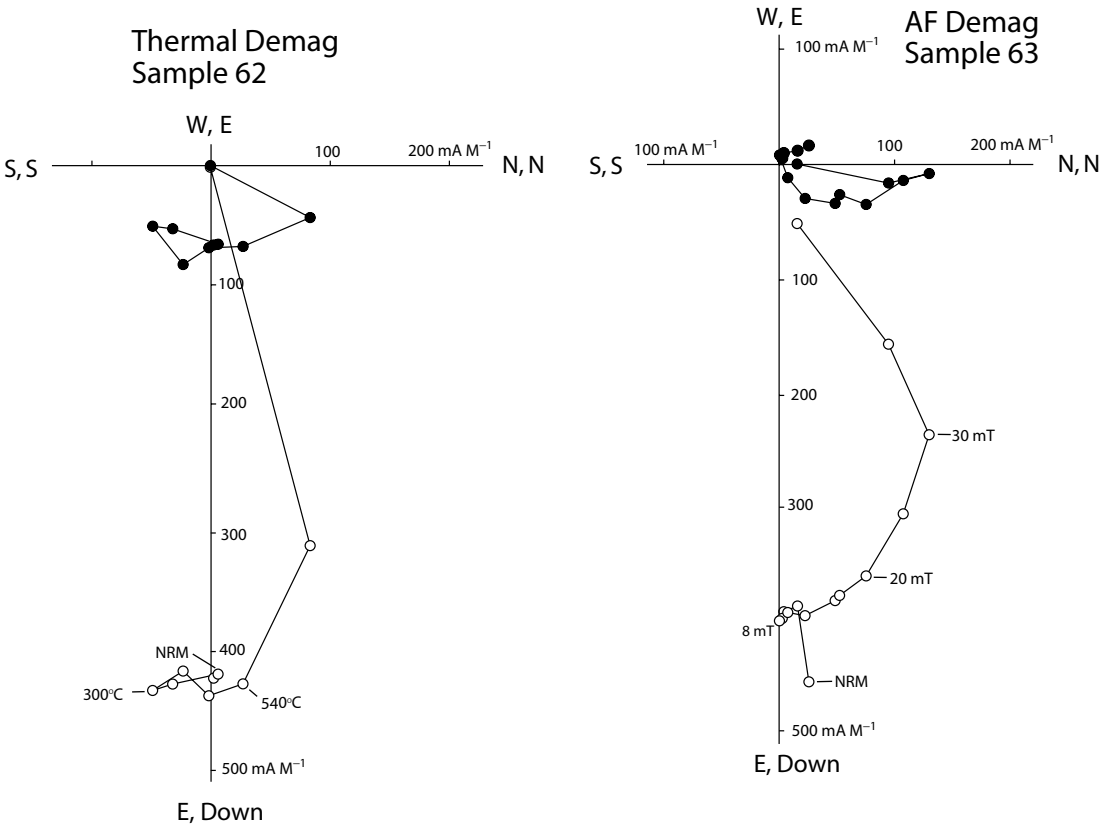

Figure 6. Thermal and AF demagnetization of dyke 4 samples.

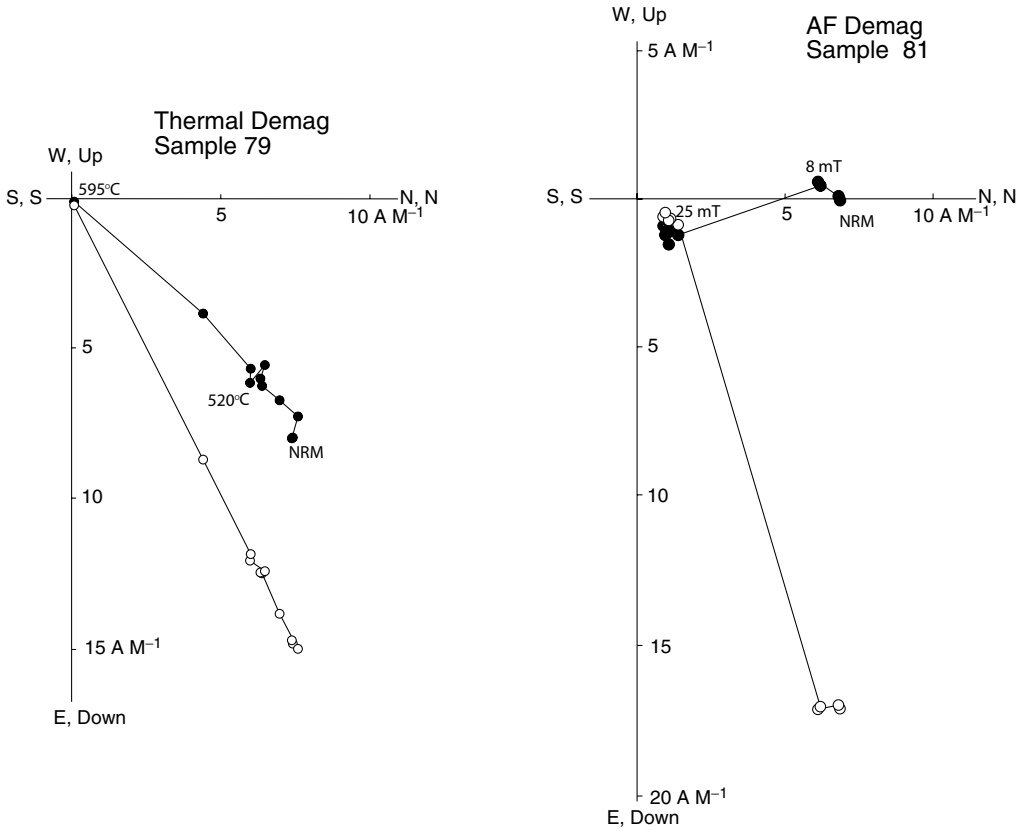

Figure 7. Thermal and AF demagnetization of dyke 5 samples. The secondary components are different for the two samples shown above; however, the ChRM directions are almost identical.

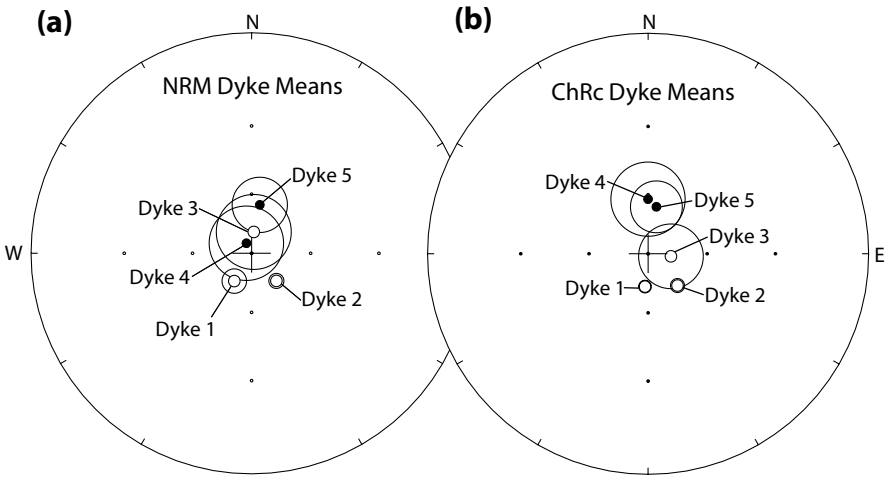

Figure 8. Dyke mean directions of (a) NRM and (b) ChRc. In the stereoplots, solid symbols indicate a positive inclination, while open symbols indicate a negative inclination. The circles are α_{95} confidence circles.

Table 2. Mean characteristic magnetization directions of each dyke, as well as mean magnetization directions for normally and reversely polarized dykes and a combined mean from all dykes (reversed dykes were inverted) after demagnetization.

Site (Polarity) $^{40}Ar/^{39}Ar$ Age	N	Dec.(°)	Inc.(°)	α_{95}	k
Dyke 1 (Normal) 1649 ± 10 Ma	8	185	−73	3.2	298.54
Dyke 2 (Normal)	9	137	−68	3.5	220.51
Dyke 3 (Normal)	5	110.1	−75.9	20.1	21.84
Dyke 4 (Reversed)	3	359.9	62.2	18	48.12
Dyke 5 (Reversed)	6	10	65.6	12.8	28.19
Normal Dykes	3*	144.9	−74.4	17.3	51.63
Reversed Dykes	2*	4.6	64	12.2	421.17
Combined (R inverted)	5*	165.8	−71.3	11.8	42.78
	Pole: 8.7°N, 22°E ($dp/dm = 18/20.6°$)				

N = number of samples (* site); $\alpha_{95} = 95$ per cent confidence circle around mean direction; k = precision parameter; mean sampling coordinates 24.5°S, 30°E.

4.2 Site 2 (dolerite dyke)

Site 2 is located along the Lydenburg road (east of the Dwars River geological monument) and exposes a ∼20-m-thick dolerite dyke in the Critical Zone of the Bushveld Complex (gabbro). The host gabbro was too weathered to drill but the magmatic layering was recorded (Table 1). High magnetic stability for the dyke samples is reflected by the almost univectorial demagnetization path, namely a single-component NRM with steep upward-dipping inclination and a SE declination (Figs 3 and 8b; dyke 2, samples 21 and 24). AF and thermal demagnetization provided identical directional results and the maximum unblocking temperature is ∼580°C.

4.3 Site 3 (dolerite dyke and host norite)

Site 3 exposes a 2-m-thick dolerite dyke in a river cutting near the Dwars River monument. The dyke has been hydrothermally altered and thin shear zones along the margin contain quartz infill. The dyke cuts spotted and mottled anorthosite. Because the contact of the dyke/anorthosite is fractured, it was not possible to sample the contact. Core samples were drilled between 0.3 and 7.5 m from the dyke. All dyke samples show persistent LB components, randomized at around 500°C, but they are randomly oriented. The HB components are similar to that of dyke 2, with a steep upward-pointing inclination and SE to E declination (Figs 4 and 8b; dyke 3, samples 37 and 33). AF demagnetization suggests overlapping coercivity spectra between LB and HB components, as indicated by the curved demagnetization trajectory (Fig. 4). The maximum available AF field of 90 mT did not completely demagnetize the sample. Maximum unblocking temperatures of ∼580 °C (as for dykes 1–2) suggest pure magnetite as the prime remanence carrier.

The NRM of the anorthosite samples close to the dyke had higher values (0.2 A m^{-1}) than those further from the dyke (0.5 mA m^{-1}); there was no change in susceptibility. The baked anorthosite host rock (0.3 m away from the dyke) showed high magnetic stability with almost univectorial behaviour (Fig. 5). This was close to the HB component in the dyke (compare Figs 4 and 5). Directional similarity and NRM intensity increase towards the dyke contact and attest to a semi-conclusive contact test. Anorthosite samples furthest from the dyke had a random distribution of HB components.

4.4 Site 4 (dolerite dyke and host norite)

Site 4 exposes a 4-m-thick dolerite dyke cutting Bushveld norite on the northwestern edge of Serafa Hill (Paschaskraal Farm). The dyke shows minor, but randomly oriented, LB components. HB components from the dykes show a steep, downward-dipping inclination with a northerly declination (Fig. 6; dyke 4, samples 62 and 63). Maximum thermal unblocking temperatures for the dyke were 565–580°C. Norite samples (sampled 3 m away) are randomly distributed in their LB and HB components.

4.5 Site 5 (dolerite dyke and host norite)

Site 5 consists of a dyke exposed as small blocks (1-m-thick surface exposure) cutting through Bushveld norite on one of the foothills to the northwest of Serafa Hill (Paschaskraal Farm). High magnetic stability for the dyke samples is reflected by almost univectorial demagnetization behaviour (Fig. 7; dyke 5, samples 79 and 81), namely a steep downward-dipping inclination with a NNE declination. The two examples in Fig. 7 indicate that some samples have LB components but they are random in direction. Maximum unblocking temperatures for the dyke were 565–580°C. Once again the norite samples (1 m from dyke) show scattered LB and HB components.

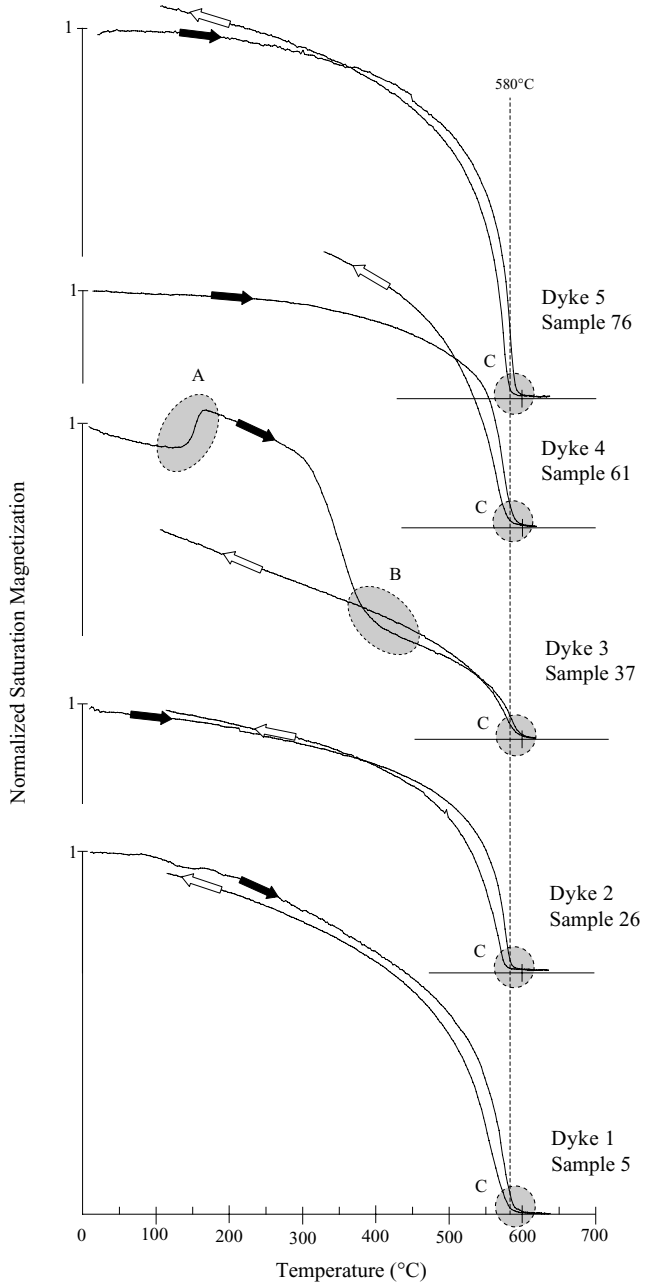

Figure 9. Thermomagnetic analysis of all dykes. Black arrows indicate the heating phase, while white arrows indicate the cooling phase. The grey patches indicate phase changes or Curie temperatures. (A) Irreversible creation of a magnetic phase with higher saturation magnetization at 150–180°C, (B) inversion of maghemite to a weaker magnetic phase at ≈350°C, and (C) Curie temperature for magnetite at ≈580°C.

5 MAGNETOMINERALOGY

All dyke samples show maximum unblocking temperatures of 565–580°C and Curie temperatures of ∼580°C (Fig. 9), thereby suggesting magnetite or Ti-poor titanomagnetite (TM) as the prime remanence carrier. However, the dykes differ slightly in their thermomagnetic (Fig. 9) and petrographic characteristics.

(1) Dyke 1. The Curie curves are almost reversible, indicating a mineralogy of magnetite, except for a small decrease in the saturation magnetization during cooling, which probably indicates that some oxidation occurred during heating and cooling. Petrographically, the opaque mineralogy is dominated by magnetite but some grains contain lamellae of ilmenite. The latter attests to high-temperature deuteric oxidation during late-stage crystallization of the dyke.

(2) Dykes 2 and 5. The Curie curves show a slight increase in saturation magnetization during cooling, indicating secondary production of magnetite. Petrographic investigation (dyke 2) shows the dominance of magnetite with lamellae of ilmenite. Dyke 5 is dominated by pure magnetite, with a minority of grains having lamellae of ilmenite.

(3) Dyke 3. Upon heating, the saturation magnetization first increases at 150–170°C followed by a distinct decrease at ∼350°C, and finally a Curie temperature at ∼580°C. The kink at 150–170°C is a typical low-temperature titanomagnetite (maghemitization) phenomenon (Ade-Hall *et al.* 1971), possibly related to hydrothermal alteration. The decrease at 350°C is probably related to the inversion of maghemite. The Curie curves suggest a combination of magnetite/TM and maghemite, the latter explaining the high-coercivity phases noted during AF demagnetization (Fig. 4; right-hand diagram). Petrographically, the opaque mineralogy of the dyke is dominated by highly altered magnetite—the majority of the alteration mineral could not be determined as grain sizes were smaller than the optical resolution. However, some alterations were identified as haematite; this could also explain the high resistance to AF demagnetization.

(4) Dyke 4. The Curie curves indicate an increase in saturation magnetization during cooling, implying production of secondary magnetite, probably from a non-magnetic phase. Petrographically, magnetite is the dominant opaque mineral and some grains show small amounts of alteration.

6 ^{40}Ar/^{39}Ar GEOCHRONOLOGY

Four samples were analysed using single- and multi-grain laser fusion (see Appendix 1 for analytical procedures). All four samples yielded Precambrian ages (Table 3, Figure 10) but only one of the samples (13—Dyke 1) yielded a set of consistent ages representing a majority of the radiogenic ^{40}Ar gas released from the analysed grains (Fig. 10a). Most of the apparent ages for this sample lie between ∼1560 and 1720 Ma, and a simple mean of the most concordant of these ages, 1649 ± 10 Ma, is within uncertainty of the total fusion age (1643 ± 10 Ma) for the sample. This is the only age from the samples analysed that can be interpreted geologically either as a crystallization age, or a post-crystallization age indicative of partial to complete resetting of an older crystallization event. On the basis of these data alone, resetting of an initially older dyke due to a 1650 Ma thermal event is indistinguishable from an initial 1650 Ma crystallization age.

The other three samples [32 (dyke 2), 70 (dyke 4) and 86 (dyke 5)] yielded variable ranges of Precambrian apparent ages (Table 3) that could not be interpreted with simple geological histories (Fig. 10b). These three rocks are clearly not Bushveld age, and all apparent ages older than Bushveld can be interpreted directly as the result of complications from excess argon. A majority of the ages from these three samples cluster in the same range as those for sample 13 (Fig. 10b; *ca.* 1400–1750 Ma), but other apparent ages obtained from the samples scatter between 1000 and 1250 Ma, with a few in the range 1875–1950 Ma. This variation obviously makes interpretation of a single magmatic event impossible to decipher and no geological interpretation was made for these three samples. No

Table 3. $^{40}Ar/^{39}Ar$ data for laser fusion experiments on single grains from four plagioclase samples.

$^{40}Ar/^{39}Ar$	$^{38}Ar/^{39}Ar$	$^{37}Ar/^{39}Ar$	$^{36}Ar/^{39}Ar$	^{39}Ar	$F^{39}Ar^{1}$	%40*[2]	$^{40}Ar^{*}/^{39}Ar_{K}$	Age (Ma)	$\pm 1\sigma$
13 plagioclase (Dyke 1)			J = .0060520						
268.634	0.018	3.816	8.094	3.089	1.12	99.6	267.63	1738.36	4.35
266.549	0.014	1.950	12.475	6.333	3.42	98.9	263.55	1721.27	1.26
231.938	0.011	1.567	4.204	14.271	8.61	99.7	231.18	1579.61	3.08
241.852	0.007	4.564	8.202	21.336	16.36	99.6	240.95	1623.56	0.87
236.078	0.011	2.355	6.456	19.672	23.50	99.5	234.93	1596.58	1.52
246.580	0.005	1.229	2.577	27.550	33.51	99.9	246.21	1646.79	2.09
247.930	0.008	0.558	3.402	35.272	46.32	99.7	247.09	1650.62	1.65
249.960	0.005	1.003	2.027	41.437	61.37	99.9	249.68	1661.94	1.71
248.752	0.007	2.577	3.946	23.313	69.84	99.9	248.46	1656.59	2.00
245.358	0.001	1.083	1.980	30.807	81.03	99.9	245.12	1641.97	3.40
244.507	0.001	0.977	4.541	32.592	92.87	99.6	243.47	1634.71	1.68
252.097	0.002	0.430	2.291	19.640	100	99.8	251.54	1670.01	2.05
86 plagioclase (Dyke 5)			J = .0060500						
256.620	0.039	6.113	41.983	0.667	1.81	96.0	246.30	1646.82	10.24
351.867	0.038	12.951	101.040	0.495	3.15	93.1	327.65	1972.36	17.60
250.363	0.061	8.515	38.111	1.050	6.00	96.7	241.98	1627.76	7.37
219.632	0.037	1.446	7.442	1.478	10.01	99.2	217.86	1517.55	5.46
302.018	0.001	0.001	0.574	0.174	10.48	99.9	301.82	1875.21	14.33
392.834	0.000	0.000	25.990	0.269	11.22	98.0	385.13	2171.44	26.56
262.963	0.043	22.905	38.158	0.655	12.99	98.9	259.94	1705.67	9.44
248.335	0.017	0.000	54.210	0.498	14.34	93.5	232.29	1584.28	9.09
203.050	0.003	0.000	11.105	0.360	15.32	98.4	199.74	1430.11	9.86
225.009	0.063	3.985	33.595	3.185	23.97	96.1	216.30	1510.19	3.06
363.516	0.085	18.378	62.290	0.787	26.10	97.3	353.66	2065.18	21.07
281.587	0.078	8.223	43.863	2.759	33.59	96.5	271.68	1754.81	5.07
169.073	0.036	6.664	18.208	2.856	41.34	97.8	165.37	1251.60	4.68
218.428	0.010	9.617	16.612	3.732	51.46	99.1	216.50	1511.15	3.07
202.136	0.036	5.699	9.109	1.537	55.63	99.5	201.10	1436.83	6.01
284.323	0.057	13.094	57.799	1.384	59.39	95.7	272.13	1756.67	7.61
268.635	0.013	15.323	38.450	0.624	61.08	97.8	262.84	1717.91	23.69
209.279	0.033	0.757	11.150	4.215	72.52	98.5	206.18	1461.69	3.44
273.288	0.045	41.345	59.510	0.907	74.98	99.2	271.15	1752.62	9.08
242.924	0.093	13.145	42.877	5.224	89.16	96.6	234.61	1594.78	1.91
257.693	0.052	5.703	28.227	1.453	93.10	97.5	251.33	1668.73	4.56
203.927	0.029	0.487	10.440	1.245	96.48	98.5	200.96	1436.12	5.75
275.584	0.061	2.028	49.365	1.296	100	95.0	261.71	1713.13	4.57
32 plagioclase (Dyke 2)				J = .0060460					
332.694	0.014	3.124	24.619	22.178	17.46	98.2	326.75	1968.29	1.17
528.797	0.027	8.708	51.588	0.853	18.13	98.2	519.20	2564.05	10.67
310.308	0.021	2.722	20.024	14.482	29.53	98.4	305.49	1888.55	4.84
450.504	0.045	4.021	31.460	13.605	40.24	98.4	443.46	2352.40	3.01
467.357	0.041	4.916	42.118	10.969	48.87	97.9	457.75	2394.28	2.11
506.482	0.054	19.614	51.464	3.342	51.50	99.5	503.70	2522.70	5.36
402.555	0.026	4.078	35.238	7.407	57.33	97.9	394.20	2200.12	2.87
524.107	0.037	6.878	40.543	5.747	61.85	98.6	516.56	2557.07	6.75
312.923	0.025	1.764	22.796	30.531	85.89	98.1	306.89	1893.92	5.89
440.396	0.053	5.043	33.696	3.947	88.99	98.4	433.21	2321.76	2.70
580.822	0.029	1.676	44.404	13.985	100	97.9	568.86	2690.44	2.32
70 plagioclase (Dyke 4)				J = .0060430					
131.878	0.069	17.997	17.092	8.308	6.15	99.1	130.7	1050.76	1.81
219.110	0.023	46.251	18.424	2.008	7.63	104.4	228.75	1566.94	7.26
211.316	0.119	53.950	28.733	5.255	11.52	104.1	219.89	1525.91	2.20
226.097	0.058	23.347	24.843	7.849	17.33	100.1	226.29	1555.65	2.61
205.948	0.137	37.636	23.863	5.029	21.06	102.2	210.39	1480.86	3.13
155.282	0.074	27.447	15.328	4.893	24.68	101.4	157.50	1207.11	2.33
262.587	0.114	7.347	19.583	29.975	46.86	98.8	259.43	1702.19	1.96
243.600	0.059	32.414	31.334	3.638	49.55	100.8	245.51	1642.10	4.03
138.785	0.058	27.528	17.246	13.511	59.55	100.8	139.91	1106.05	1.21
78.885	0.044	15.021	9.126	13.369	69.45	99.6	78.54	701.07	2.46
249.564	0.171	28.784	24.941	4.691	72.92	101.1	252.33	1671.80	3.64
144.475	0.148	22.323	19.019	9.464	79.92	99.7	144.00	1130.04	1.44
199.106	0.130	38.162	25.354	6.074	84.42	101.9	202.95	1444.77	2.86
126.058	0.161	24.194	16.372	6.169	88.98	100.2	126.32	1023.85	2.06
138.259	0.101	24.627	14.512	14.884	100	100.9	139.53	1103.75	2.26

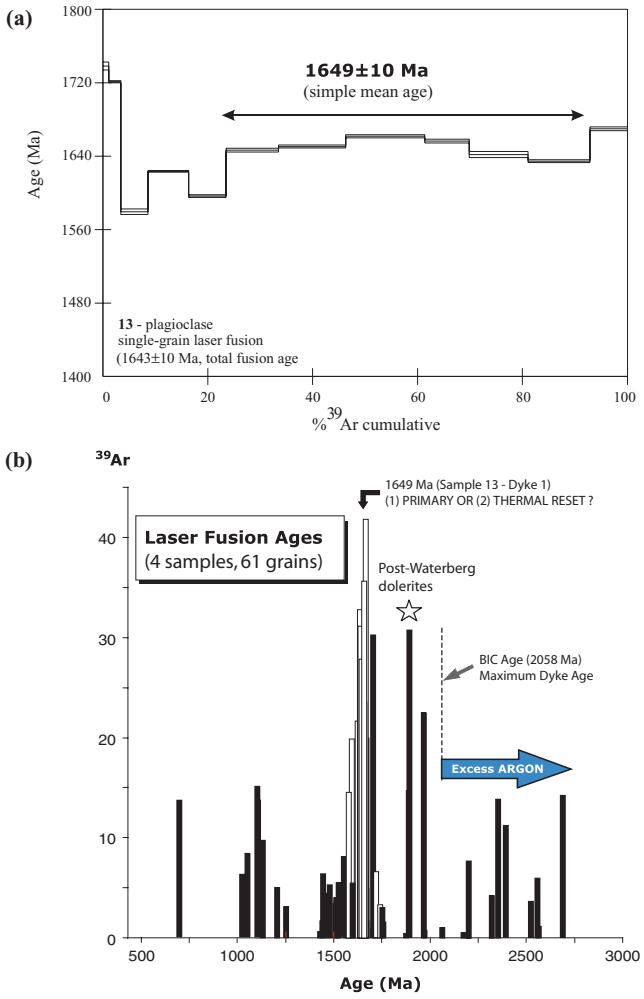

Figure 10. (a) Single-grain laser fusion of sample 13 (dyke 1). (b) All laser fusion ages plotted against the amount of ^{39}Ar (Table 3) released during the experiment; this is taken as a rough proxy to K-content of the plagioclase grains. Open symbols are data from sample 13; remaining samples are shown as solid rectangles. No consistent correlation was observed between gas volume released in the experiment, K-content and age, although the higher, relative K steps of sample 13 appear to yield the most consistent ages. A post-crystallization resetting event (see text for discussion) would have had less effect on the Ar content of higher-K plagioclase grains than on relatively lower-K plagioclase grains. Inverse isochron analysis, which often yields information with regard to the presence of excess Ar, was not applicable to these samples because of the very radiogenic yields for all fusion steps. The age of post-Waterberg dolerites (1872–1879) is indicated as a star.

consistent correlation was found between experimental gas volume released, K-content (proxy from ^{39}Ar values for each fusion step), or number of grains fused in each step (range from one to five grains per fusion step per sample). The variation in ages is thus attributed to a combination of geological and laboratory effects including excess argon (ages older than Bushveld), partial resetting of original crystallization ages and incomplete outgassing during laser fusion. The cause of the partial resetting of original crystallization ages has clearly affected the Ar content and distribution in the samples, but the nature of the resetting was not thermally significant enough to affect the remanent magnetic signature (see also below).

7 FIELD STABILITY TESTS

Two reversal tests were implemented in order to determine if the reversely polarized dykes (sites 4–5) were of similar age to the normally polarized dykes (sites 1–3). It was found that the dykes shared a common mean at 95 per cent confidence according to the method of McFadden & Lowes (1981). The reversal test of McFadden & McElhinny (1990) also indicated a positive reversal test with a C classification (i.e. the angle between the reversals is between 170° and 160°; critical angle = 19.5°; observed angle = 17°). Dual-polarity dykes (as also clearly seen from magnetic maps since remanent magnetization is dominant; see Q-factors in Table 1) and a semi-conclusive contact test from site 3 clearly argue for a primary magnetization.

ChRc values from the host rock are very scattered, and correcting for magmatic layering (typically dipping 10°–15°) does not statistically improve the grouping, and host-rock HB components are not evaluated. In order to test whether the host rock has been tilted after dyke intrusion, dyke site means were corrected for magmatic layering in the host rock. The clustering of the dykes, however, decreases when corrected for magmatic layering (k decreased from 42.8 to 37.6), but the test was statistically insignificant at the 95 per cent confidence level.

8 AGE OF REMANENCE

Since reverse and normal polarity dyke means (Fig. 8b) share a common mean at the 95 per cent confidence level, HB components were inverted to the same polarity and yielded a combined mean remanence direction with a declination of 165.8°, inclination of −71.3°, and a pole position with latitude 8.7°N and longitude 22°E (Table 2).

The studied dykes have been assumed (e.g. Uken & Watkeys 1997) to be of Karroo (Jurassic) age, but the pole position clearly does not resemble any Karroo poles (Fig. 11c). On the contrary, the pole position overlaps with major geological events at around 2 Ga, i.e. the 2058.9 ± 0.8 Ma BIC that they intrude. BIC poles show a clear NNE polar distribution that may indicate that all magmatic phases are not of identical age, or that the data have been affected by postmagmatic structural corrections and/or inadequate demagnetization procedures. Our dyke mean pole statistically overlaps with data for the various BIC Zones (except the Merensky Reef), the ∼1.9 Ga Waterberg–Southpansberg magmatic event (Hanson *et al.* 2004) and the 1875 Ma (but poorly dated) Sand River dykes (Fig. 11a). Based on the pole position, the dykes therefore suggest an emplacement age of ∼1.9 to ∼2 Ga (maximum age = 2058 Ma). Hanson *et al.* (2004) combined well-dated post-Waterberg dolerites (1872–1879 Ma) with Soutpansberg mafic rocks due to similar palaeomagnetic results. Note, however, that Waterberg and Southpansberg have opposite polarities whilst the dykes from this study have dual polarities that match both Waterberg and Southpansberg.

Only dyke 1 (sample 13) provided a reliable ^{40}Ar/^{39}Ar age. The age, of 1649 ± 10 Ma, however, is approximately 250 Myr younger than the age estimated from the palaeomagnetic comparison above. Whilst the magnetizations are primary, it is more problematic to establish if the ^{40}Ar/^{39}Ar plagioclase age represents (1) a 1650 Ma crystallization age or (2) a complete or partial resetting of an initially older dyke caused by a younger thermal event.

Alternative 1

If the dykes are 1650 Ma, then the pole position is identical to ∼1.9–2 Ga poles and represents the crossover point of an apparent polar

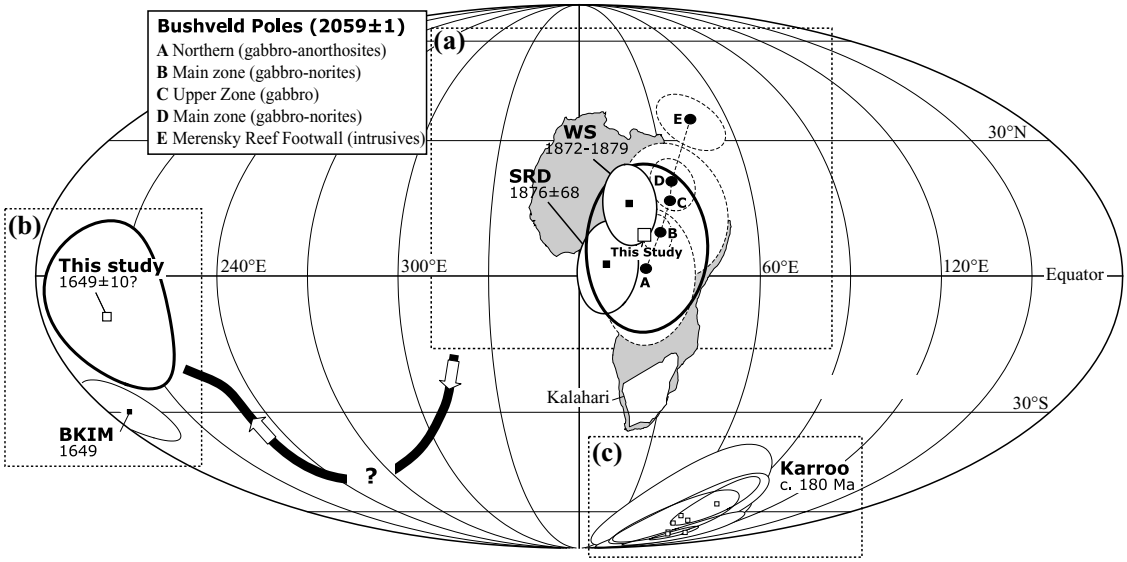

Figure 11. (a) Palaeomagnetic pole positions from the Bushveld Igneous Complex (solid dark circles denoted A to E; Hattingh 1986a,c, 1989; Hattingh & Pauls 1994), Waterberg–Southspans magmatic event (WS, Hanson *et al.* 2004) and Sand River Dykes (SRD; Morgan 1985) compared with our mean dyke pole (open square). There are other poles that fall in the area of our mean dyke pole but we do not include poles older than Bushveld (maximum age for the dykes) or poles that do not represent primary magnetizations (see Evans *et al.* 2002, for review). (b) Alternative comparison of our mean dyke pole with poles of younger ages due to the ^{40}Ar-^{39}Ar age of 1649 ± 10 Ma (reversed polarity in diagram for reasons of simplicity). Our pole is compared with the 1649 Ma Bathlaros Kimberlite (BKIM) pole of Hargraves (1989). (c) The studied dykes have been argued to be of Jurassic age. Shown for comparison are Karroo-aged poles from South Africa (upgraded from Torsvik & Van der Voo 2002), which are very different from the pole derived from the studied dykes. All poles are shown with dp/dm confidence ellipses except for pole WD (A95). Mollweide projection.

wander (APW) loop, the pole is of opposite hemispheric polarity (i.e. North versus South pole), or alternatively no APW between ∼2 Ga and 1650 Ma. For reasons of diagrammatic simplicity we plot our mean dyke pole with opposite polarity in Fig. 11b and compare it with the only pole of similar age that plots in the vicinity of our mean pole. However, the 'reference' pole (Bathlaros kimberlite) is of limited scientific value—the pole is based on only seven samples (one site), the data are not documented in diagrammatic form (only listed in table 2 of Hargraves 1989), and the age of 1649 Ma is based on Rb/Sr with no published errors. From South Africa it is therefore not possible to find high-quality and well-dated palaeomagnetic poles that can corroborate a 1650 Ma remanence age for the dykes.

Alternative 2

If the dykes are ∼1.9 Ga, as indicated from palaeomagnetic data, then the ^{40}Ar/^{39}Ar age must represent a thermal resetting event. In the authors' experience, primary palaeomagnetic signatures and reset (younger) ^{40}Ar/^{39}Ar mineral ages (plagioclase, biotite, feldspar) are rare, but have been observed (e.g. Nysæther *et al.* 2002). In the current case, the most stable remanence is carried by high-temperature, deuterically oxidized titanomagnetites that may have survived moderate thermal events. Dyke samples are commonly characterized by low-temperature components, and the primary high-temperature components are commonly identified at temperatures above 500–530°C (see dyke examples in Figs 2, 4 and 6)—this may be indicative of a thermal overprint that can explain a reset ^{40}Ar/^{39}Ar age. However, other samples are of almost single-component nature (e.g. dyke 2 samples; Fig. 3), and the gross similarity in NRM and ChRc mean directions (Fig. 8) does not suggest major magnetic overprinting.

9 CONCLUSIONS

Palaeomagnetic data from dykes intruding the eastern BIC are of good quality and high Q factors (average = 11.4) and testify to the importance of remanent magnetization for magnetic modelling of the dykes. The prime remanence carriers are pure magnetite and deuterically oxidized titanomagnetites. Dykes show both normal and reversed polarities, and positive reversal tests suggest that the dykes are related to the same magmatic event. Our results indicate that the magnetization is primary, and that secular variation has been averaged out. Dyke site means, when corrected for magmatic layering in the host rocks, show insignificant changes at the 95 per cent confidence level, and it therefore remains unclear whether the dykes were emplaced before, during or after tilting of the host rocks.

The dykes, recognized as prominent magnetic NE–SW lineaments on aeromagnetic maps (Fig. 1c), are not of Karroo but of Proterozoic age. A comparison with palaeomagnetic poles from South Africa (notably Waterberg–Southpansberg) suggests an intrusion age of ∼1.9 Ga (maximum age of 2058 Ma, the age of the BIC that they intrude), and that the Kalahari Craton was located at relatively high (>50°) southerly (or northerly) latitudes during dyke emplacement. The 1649 ± 10 Ma ^{40}Ar/^{39}Ar plagioclase age from one dyke is probably a reset ^{40}Ar/^{39}Ar age.

ACKNOWLEDGMENTS

Financial support for this study was provided by Anglo Platinum, the National Research Foundation (South Africa), the Academy of Sciences & Statoil (VISTA) and the Norwegian Research Council.

REFERENCES

Ade-Hall, J.M., Palmer, H.C. & Hubbar, T.P., 1971. The magnetic and opaque petrological response of basalt to regional hydrothermal alteration, *Geophys. J. R. astr. Soc.,* **24,** 137–174.

Ashwal, L.D., Webb, S.J. & Knoper, M.W., 2000. Physical properties of Bushveld rocks: magnetic and density profiles in the Bellevue drillcore, Northern Lobe, Workshop on the Bushveld Complex: Gethlane Lodge, Burgersfort, abstr, 4–5.

Buick, I.S., Mass, R. & Gibson, R., 2001. Precise U-Pb titanite age constraints on the Bushveld Complex, South Africa, *J. geol. Soc. Lond.,* **158,** 3–6.

Crow, C. & Condie, K.C., 1990. Geochemisrty and origin of early Proterozoic volcanic rocks from the Transvaal and Soutpansberg successions South Africa, *Precamb. Res.,* **47,** 17–26.

Duffield, W.A. & Dalrymple, G.B., 1990. The Taylor Creek rhyolite of New-Mexico—A rapidly emplaced field of lava domes and flows, *Bull. Volc.,* **52,** 475–487.

Eales, H.V., Marsh, J.S. & Cox, K.G., 1984. The Karoo igneous province: An introduction, in *Petrogenesis of the Volcanic Rocks of the Karoo Province,* pp. 1–26, ed. Erlank, A.J., Geological Society of South Africa, Johannesburg.

Evans, D.A.D., Beukes, N.J. & Kirschvink, J.L., 2002. Paleomagnetism of a lateritic paleoweathering horizon and overlying Paleoproterozoic red beds from South Africa: Implications for the Kaapvaal apparent polar wander path and a confirmation of atmospheric oxygen enrichment, *J. geophys. Res.,* **107,** 12, 2326, doi:10.1029/2001JB000432.

Hanson, R.E., Gose, W.A., Crowley, J.L., Ramezani, J., Bowring, S.A., Bullen, D.S., Hall, R.P., Pancake, J.A. & Mukwakwani, J., 2004. Paleoproterozoic intraplate magmatism and basin development on the Kaapvall Craton: Age, paleomagnetism and geochemistry of ∼1.93 to ∼1.87 Ga post-Waterberg dolerites, *S. Afr. J. Geol.,* **107,** 53–74.

Hargraves, R.B., 1989. Palaeomagnetism of Mesozoic kimberlites in Southern Africa and the Cretaceous apparent polar wander curve for Africa, *J. geophys. Res.,* **94,** 1851–1866.

Hargraves, R.B., Rehacek, J. & Hooper, P.R., 1997. Palaeomagnetism of the Karoo igneous rocks in Southern Africa, *S. Afr. J. Geol.,* **100,** 195–212.

Hattingh, P.J., 1986a. The paleomagnetism of the main zone in the western Bushveld Complex, *Earth planet. Sci. Lett.,* **79,** 441–452.

Hattingh, P.J., 1986b. The paleomagnetism of the main zone of the eastern Bushveld Complex, *Tectonophysics,* **124,** 271–295.

Hattingh, P.J., 1986c. The paleomagnetism of the Merensky Reef footwall rock of the Bushveld Complex, *Trans. Geol. Soc. S. Afr.,* **89,** 1–8.

Hattingh, P.J., 1989. Palaeomagnetism of the upper zone of the Bushveld Complex, *Tectonophysics,* **165,** 131–142.

Hattingh, P.J. & Pauls, N.D., 1994. New palaeomagnetic results from the northern Bushveld Complex of South Africa, *Precamb. Res.,* **69,** 229–240.

Hunter, D.R. & Reid, D.L., 1987. Mafic dyke swarms in Southern Africa, in *Mafic Dyke Swarms,* pp. 445–456, eds Halls, H.C. & Fahrig, W.F., Geological Association of Canada, Geological Association of Canada, *Special paper 34*.

Lee, C.A., 1996. A review of the mineralization in the Bushveld Complex and some other layered mafic intrusions, in *Layered Intrusions,* Vol. 15, pp. 103–145, ed. Cawthorn, R.G., Developments in Petrology, Elsevier, Amsterdam, The Netherlands.

McFadden, P.L. & Lowes, F.J., 1981. The discrimination of mean directions drawn from Fisher distributions, *Geophys. J. R. astr. Soc.,* **67,** 19–33.

McFadden, P.L. & McElhinny, M.W., 1990. Classification of the reversal test in palaeomagnetism, *Geophys. J. Int.,* **103,** 725–729.

Maré, L.P., Oosthuizen, B.C., Corner, B., Nkwana, M.M. & Antoine, L.A.G., 2001. *South African Geophysical Atlas,* Council for Geoscience, Pretoria.

Molyneux, T.G., 1970. The geology of the area in the vicinity of Magnet Heights, Eastern Transvaal, with special reference to the magnetic iron ore, *Geol. Soc. S. Afr., Spec. Publ.,* **1,** 228–241.

Morgan, G.E., 1985. The paleomagnetism and cooling history of metamorphic and igneous rocks from the Limpopo Mobile Belt, southern Africa, *Bull. geol. Soc. Am.,* **96,** 663–675.

Nysæther, E., Torsvik, T.H., Feist, R., Walderhaug H.J. & Eide, E.A., 2002. Ordovician Palaeogeography with new palaeomagnetic data from the Montagne Noire (Southern France), *Earth planet. Sci. Lett.,* **203,** 329–341.

Rex, D.C. & Guise, P.G., 1995. Evaluation of argon standards with special emphasis on time scale measurements, in *Phanerozoic Time Scale, 21–23. Bulletin Lias,* ed. Odin, G.S., Information, IUGS Subcomission on Geochronology 13, Trondheim, Norway.

Sharpe, M.R., 1981. Petrology and geochemistry of pre-Bushveld and Waterberg mafic sills, *Trans. geol. Soc. S. Afr.,* **84,** 75–83.

Strauss, C.A., 1947. The petrology of a small dolerite and granophyre complex in the New Belgium Block, Potgeitersrus District, *Trans. geol. Soc. S. Afr.,* **50,** 73–104.

Torsvik, T.H. & Van der Voo, R., 2002. Refining Gondwana and Pangea palaeogeography: estimates of Phanerozoic non-dipole (octupole) fields, *Geophys. J. Int.,* **151,** 771–794.

Turner, G., Huneke, J.C., Podosek, F.A. & Wasserburg, G.J., 1971. ^{40}Ar-^{39}Ar ages and cosmic ray exposure ages of Apollo 14 samples, *Earth planet. Sci. Lett.,* **12,** 19–35.

Uken, R. & Watkeys, M.K., 1997. An interpretation of mafic dyke swarms and their relationship with major mafic magmatic events on the Kaapvaal Craton and Limpopo Belt, *S. Afr. J. Geol.,* **100**(4), 341–348.

von Gruenewaldt, G., Sharpe, M.R. & Hatton, C.J., 1985. The Bushveld Complex: introduction and review, *Economic Geology,* **80**(4), 803–812.

APPENDIX A: ^{40}Ar/^{39}Ar ANALYTICAL PROCEDURES

Mineral separates were obtained using standard techniques: the rocks were crushed, washed and sieved to fraction sizes 250–180 μm (plagioclase). Before packing in Al-foil, mineral separates were hand-picked under a binocular microscope to exclude grains with visible inclusions and/or surface alteration; hand-picked material was rinsed in alternating acetone and distilled water. Sample packets were stacked and loaded in an Al-capsule for irradiation in the 5C site at the McMaster Nuclear Reactor facility, Hamilton, Canada. The samples were irradiated for 25 hr (50 MWH) with a nominal neutron flux of 4×10^{13} n cm^{-2} s^{-1}, and a temperature in the irradiation site of $<50^{\circ}$C (M. Butler, personal communication). Production of isotopes from Ca and K were determined by irradiation of CaF and K_2SO_4 salts; values of $^{36}/^{37}\mathrm{Ca} = 0.000238$, $^{39}/^{37}\mathrm{Ca} = 0.001121$, and $^{40}/^{39}\mathrm{K} = 0.02878$ were used. Neutron fluence monitors included Taylor Creek Rhyolite sanidine, Tinto biotite and Hb3gr hornblende, with ages of 27.92 Ma (TCR; Duffield & Dalrymple 1990), 410.3 Ma (Tinto; Rex & Guise 1995) and 1072 ± 11 Ma (Hb3gr; Turner *et al.* 1971), respectively. Uncertainties in J-values for monitors were usually <1 per cent, without including error in monitor age; a conservative 1 per cent error in J-value is used in the final age calculation presented in the figures and in the text. Ages in the text, figures and tables are presented at 1σ.

Samples were analysed at the ^{40}Ar/^{39}Ar Geochronology Laboratory of the Norwegian Geological Survey. Gas from irradiated samples was released by heating one to five plagioclase grains to fusion (usually into a glass bead) with a 20-W Merchantek CO_2 laser operating at infrared wavelength. To fuse grains, laser conditions of 7 Hz and 0.6–0.7 W (9–11 per cent operating power) were typically sufficient. Beam diameters used were either 250, 325 or 500 μm.

Gas released from a sample at a single temperature step was cleaned in the extraction line for 11 minutes using two pairs of SAES AP-10 getters, mounted in isolated sections of the line, each maintained with their own vacuum pumps. On each of the getter pairs, one getter was maintained at room temperature while the

other was maintained at 400°C. The purified gas was then analysed on a MAP 215–50 mass spectrometer. Pneumatic valves on both the extraction line and mass spectrometer are automated using LabView software (code written by M.O. McWilliams). Dynamic blank measurements on mass 40 indicate a stable background (2.19×10^{-14} ccSTP), barely above instrument background levels (between-mass signal levels).

Data for blanks, monitors and unknowns were collected on a Johnson electron multiplier with gain setting at 1, while the magnet was automatically scanned over masses 35 to 41 in a cycled, 'peak-hop' mode. Masses 37 to 40 were each measured in eight cycles with 10 counts per mass per cycle, with the exception of mass 36, which was measured with 20 counts per cycle. Background levels (blanks) for the laser port were measured every three to four fusion experiments. Blanks were maintained at levels of 4–5.5 $\times$ 10^{-12} ccSTP for mass 40, 1.6 $\times$ 10^{-13} ccSTP for mass 37, and $\leq$3 $\times$ 10^{-14} ccSTP for masses 39, 38 and 36.

Data from unknowns were corrected for blanks prior to being reduced with the IAAA (Interactive Ar-Ar Analysis) software package written by T.H. Torsvik and N.O. Arnaud. Data reduction in IAAA incorporates corrections for interfering isotopes, mass discrimination, error in blanks and decay of ^{37}Ar. Mass discrimination for the mass spectrometer is determined through measurement of air composition from a pneumatic pipette.